

TRACE: Structure-Aware Character Encoding for Robust and Generalizable Document Watermarking

Jiale Meng¹, Jie Zhang², Runyi Hu³, Zheming Lu¹, Tianwei Zhang³, and
Yiming Li³

¹ Zhejiang University

² CFAR and IHPC, A*STAR, Singapore

³ Nanyang Technological University

Abstract. We propose TRACE, a structure-aware framework leveraging diffusion models for localized character encoding to embed data. Unlike existing methods that rely on edge features or pre-defined codebooks, TRACE exploits character structures that provide inherent resistance to noise interference due to their stability and unified representation across diverse characters. Our framework comprises three key components: **(1)** adaptive diffusion initialization that automatically identifies handle points, target points, and editing regions through specialized algorithms including movement probability estimator (MPE), target point estimation (TPE) and mask drawing model (MDM), **(2)** guided diffusion encoding for precise movement of selected point, and **(3)** masked region replacement with a specialized loss function to minimize feature alterations after the diffusion process. Comprehensive experiments demonstrate TRACE’s superior performance over state-of-the-art methods, achieving more than 5 dB improvement in PSNR and 5% higher extraction accuracy following cross-media transmission. TRACE achieves broad generalizability across multiple languages and fonts, making it particularly suitable for practical document security applications.

1 Introduction

Documents are ubiquitous in our daily lives, appearing in various forms such as official papers, printed materials, and digital documents. Tracing their origins is critical for protecting textual content and preventing misuse. While numerous NLP-based watermarking techniques [1, 32] have been proposed to trace the provenance of text generated by large language models (LLMs), these methods are primarily designed for purely digital text and are unsuitable for many real-world scenarios. For example, they cannot protect visualized text such as printed, handwritten, artistic typography, or stamped documents, or cases where the textual content cannot be modified due to sensitivity or authenticity constraints.

Although there are many data hiding methods for color images [9, 11, 19], these techniques cannot be directly used for documents since documents are typically composed of characters and with smooth backgrounds, instead of having

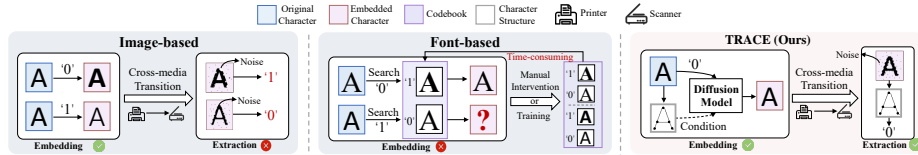


Fig. 1: Illustration of different document hiding methods. Image-based methods embed information by adjusting the proportion of black pixels but are vulnerable to noise from cross-media transmission, leading to extraction errors. Font-based methods rely on predefined character codebooks, which limits their generalizability when encountering unseen characters. In contrast, our method leverages character structures to guide diffusion-based encoding, ensuring broad applicability. Moreover, character structures are more stable to noise, providing strong robustness.

complex colors and textures. To address this problem, some researchers designed document-oriented hiding methods tailored to the characteristics of documents, mostly including image-based [16, 26] and font-based [27, 29] approaches. As shown in Fig. 1, image-based methods treat the document as an image, embedding data by altering the ratio of black and white pixels of each character. However, these methods are not robust with respect to noise introduced during cross-media transmission (*e.g.*, printing or scanning) that significantly disrupts the black-and-white pixel ratio. Besides, modifying more pixels would greatly sacrifice stealthiness, although it may improve the robustness to some extent. Font-based methods implant information by replacing the original character with its specific variant designed in a pre-defined codebook. While these methods are more robust to noise, their generalizability is limited to a large extent. This is mostly because the codebook cannot possibly include every character that might appear in a document due to the diversity of languages and fonts, a limitation that is particularly acute when encountering highly variable characters such as handwritten styles or artistic fonts. Overall, it is crucial for a document hiding method to maintain robustness, generalizability, and invisibility simultaneously. However, to the best of our knowledge, there is no prior method that can fulfill all of them. As such, an intriguing and important question arises: *Is it possible for us to design a document hiding method that simultaneously offers strong robustness, wide generalizability, and high imperceptibility?*

The answer to the aforementioned question is positive, although its solution is non-trivial. In this paper, we argue that we can implant data based on character structure encoding to meet all aforementioned requirements. Intuitively, character structures are less susceptible to noise interference since it is more stable; the structure can be regarded as a skeleton consisting of keypoints and connecting lines (see Fig. 1), thus providing a unified representation across diverse characters; it can also ensure stealthiness since modifying a few pixels around the structure will not change its appearance.

To do so, we propose a structure-based glyph modification method for document hiding (dubbed ‘TRACE’), inspired by Dragdiffusion [20]. In general, our

TRACE exploits keypoints to guide diffusion models to generate encoded characters by moving specific keypoints (*i.e.*, handle points) to their corresponding target positions. Specifically, the information embedding stage consists of three main steps: **(1)** adaptive diffusion initialization (ADI), **(2)** guided diffusion encoding (GDE), and **(3)** masked region replacement (MRR). For the first step, the key elements guiding the diffusion process are determined, including handle point, target point, and editing region, through a systematic process involving the motion probability estimator (MPE), target point estimation (TPE), and mask drawing module (MDM), respectively. The MPE adaptively computes a score for each keypoint and selects the point with the highest score as the handle point, where a higher score indicates greater motion probability. Subsequently, the TPE determines the target point based on the directional properties of the stroke containing the handle point, ensuring watermark embedding while preserving the structural consistency of the character. MDM adaptively defines the editing area based on the handle point and target point, significantly enhancing the precision of the embedding operation. Upon obtaining the key elements, GDE exploits DragDiffusion to generate the encoded character. In particular, to minimize feature alterations in non-edited regions caused by the diffusion process, we introduce a simple yet effective technique (*i.e.*, MRR), which replaces the content in the masked region of the original image with corresponding content from the edited image. Concurrently, we formulate a specialized loss function to ensure feature consistency within the masked region before and after editing, thereby preserving the perceptual integrity of the encoded character while maintaining the validity of the embedded data.

In summary, our main contributions are three-fold. **(1)** We propose a novel paradigm by embedding information into character structures, achieving a better balance between robustness, generalizability, and imperceptibility. **(2)** We design a structure-guided hiding scheme and a simple yet effective method (*i.e.*, ‘TRACE’) by leveraging diffusion models. **(3)** Extensive experiments are conducted, which verify the robustness, generalizability, and invisibility of our method, and its resistance to potential attacks. We hope our method can provide new insights into document hiding, to facilitate trustworthy document sharing and leakage attribution.

2 Related Work

2.1 Hiding Information in Documents

Font-based Methods [18, 22, 27, 29, 31]. Xiao et al. [27] gathered volunteers to select the glyphs most similar to the original font from a set of glyph variants. This process was repeated for different fonts to construct a glyph codebook. [18] generated character variants by adjusting the position of character strokes. Both methods, however, rely heavily on manual participation to construct the codebook, which makes them impractical. To address this, Yang et al. [29] made some improvements by proposing a two-stage learning framework that automatically generates encoded characters. Although this method eliminates the need

for manual intervention in constructing the character codebook, it does not fundamentally address the issue of generalizability. For example, when encountering glyphs that have not been pre-trained, this method still cannot succeed.

Image-based Methods [11, 13, 16, 23, 26, 30]. Following Wu et al.’s [26] foundational work on pixel flipping score calculation, many subsequent methods embed information by flipping pixels to establish a relationship between the embedded data and black pixel statistical features. However, these methods are sensitive to the noise introduced during cross-media transmission, which can disrupt pixel features and significantly degrade robustness.

Format-based Methods [3, 4, 10, 35]. These methods typically embed watermarks by adjusting the spacing between lines or words, which generally suffer from low embedding capacity and poor robustness [3]. Additionally, some approaches require the original document for data extraction, posing significant challenges for practical applications.

Linguistic-based Methods [6, 7, 12, 28]. This approach conceals data by modifying textual syntactic and semantic properties. However, such content alterations are generally prohibited for critical documents like contracts and confidential files, thereby limiting the generalizability of the method.

More discussions and comparisons are in Appendix K.

2.2 Diffusion-based Image Editing

Diffusion models [8, 17] have garnered significant attention for their high-quality generation capabilities. Research has leveraged these models for image editing through prompt-based [14, 33, 34] and point-based approaches [15, 20, 21]. Prompt-based methods enable image manipulation via textual prompt modifications but typically lack spatial precision. Conversely, point-based techniques facilitate targeted adjustments in specific regions via point-to-point transformations. To our knowledge, no prior work has explored diffusion-based image editing for watermarking applications.

3 Methodology

In general, our TRACE has two main stages: data embedding and data extraction. The embedding stage consists of three steps: **1)** adaptive diffusion initialization, **2)** guided diffusion encoding, and **3)** masked region replacement. Fig. 2 shows the embedding framework of TRACE.

3.1 Threat Model

This paper considers two primary entities: the document owner and an adversary. Following prior works on text watermarking [29, 30], the adversary is assumed to redistribute watermarked documents without authorization through cross-media channels (*e.g.*, print-scan workflows, print-camera capture, and screenshots).

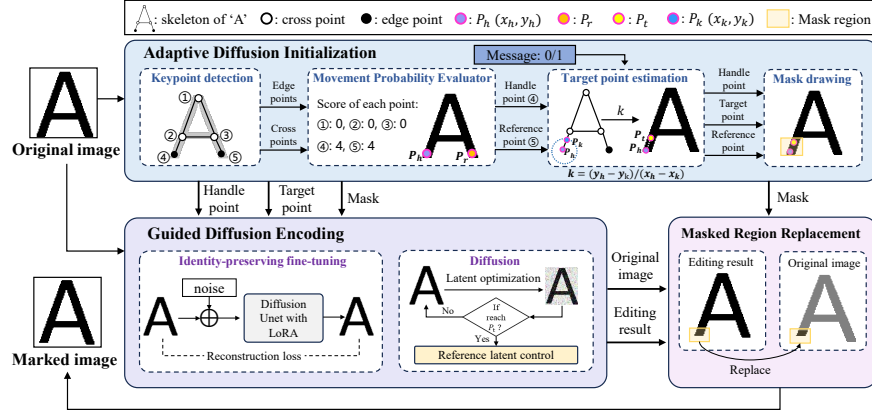


Fig. 2: TRACE Embedding Pipeline. **Step 1. Adaptive Diffusion Initialization:** Handle points, target points, and masks are identified to guide the subsequent diffusion process. **Step 2. Guided Diffusion Encoding:** The diffusion model’s UNet is fine-tuned via LoRA to better capture original image features. The marked image is then generated by controlled movement of handle points to target points within the predefined mask region. **Step 3. Masked Region Replacement:** The content within the mask of the original image is replaced with the corresponding encoded segments.

The documents may exhibit diverse formats, including multiple font families and sizes, multilingual scripts, handwritten text, and artistic or stylized typography. In general, the document owner aims to ensure that watermark extraction remains robust after such cross-media transmission, thereby enabling reliable provenance tracing and copyright protection in real-world scenarios. We also assume that the adversary may know the high-level design of our method but cannot access the specific embedding parameters used by the document owner, and may attempt to devise adaptive attacks to bypass the watermark.

3.2 Adaptive Diffusion Initialization

As shown in the blue area of Fig. 2, in this stage, given a text image I_{cover} , we first extract endpoints and junction points from its skeleton I_{ske} , which are then fed into the movement probability evaluator (MPE) to select the handle point P_h and its reference point P_r . Subsequently, the MPE outputs are used to calculate the target point P_t according to the message. Finally, both P_h and P_t are processed by the mask drawing module (MDM) to generate the mask \mathcal{M} .

Keypoint Detection. As shown in Fig. 2, to guide the diffusion-based editing process, we first extract character keypoints, which are categorized into two distinct types: endpoints and junction points, denoted by sets E and C , respectively. Our keypoint extraction network builds upon the lightweight OpenPose architecture [5], by selectively retaining only the keypoint computation components while eliminating elements related to keypoint matching and grouping. Moreover, we modify the output confidence map to comprise three channels: an

endpoint heatmap, a junction point heatmap, and a background heatmap. Note that the keypoint extraction methodology is flexible and user-defined, allowing seamless integration of improved detection techniques.

Movement Probability Evaluator. After identifying junction points and endpoints, we select the optimal point to serve as the handle point for manipulation. The movement probability evaluator (MPE) automates this selection process for each unique character, which enhances extraction efficiency while maintaining the visual consistency of characters before and after encoding.

Before delving into the operating mechanism of MPE, we first introduce a critical component: the reference point P_r . MPE utilizes P_r as a reference to determine the handle point P_h . For each point p_i^e in set E with coordinates (x_i^e, y_i^e) , the reference point $p_{i,j}^r$ with coordinates $(x_{i,j}^r, y_{i,j}^r)$ is defined as a point in $E \setminus \{p_i^e\} \cup C$. Additionally, $x_{i,j}^r$ falls within the interval $[x_i^e - \tau, x_i^e + \tau]$ and $y_{i,j}^r$ within $[y_i^e - \tau, y_i^e + \tau]$, where $\tau \in \mathbb{Z}^+$. In particular, MPE only considers endpoints as potential P_h , excluding junction points where multiple strokes converge, as manipulating these would compromise character structural integrity. Each endpoint p_i^e is associated with multiple reference points $p_{i,j}^r$, collectively denoted as $R_i = \{p_{i,j}^r \mid 0 \leq j \leq m\}$, where m represents the cardinality of $E \setminus \{\pi^e\} \cup C$. After establishing R_i for each endpoint p_i^e , MPE assigns a score $s_{i,j}$ to each $p_{i,j}^r$ in R_i , based on specific rules below, which are recorded as triplets $(p_i^e, p_{i,j}^r, s_{i,j})$. A higher score $s_{i,j}$ indicates a greater suitability of p_i^e as the handle point. The p_i^e associated with the highest score $s_{i,j}$ is designated as P_h , with its corresponding $p_{i,j}^r$ established as the reference point P_r for P_h .

We hereby describe our scoring rules. For an endpoint p_i^e with $|R_i| = 0$ (no reference point), the score is set to 0. When $|R_i| > 0$, each $p_{i,j}^r$ receives an initial score of 1. MPE evaluates each pair $(p_i^e, p_{i,j}^r)$ by analyzing their connectivity, determining whether they lie on the same stroke. If p_i^e and $p_{i,j}^r$ share the same stroke (denoted as $p_i^e \sim p_{i,j}^r$), the score remains unchanged; otherwise, it increases by one. When multiple $p_{i,j}^r$ s achieve a score of 2, an additional point is awarded to $p_{i,j}^r$ with the smallest y-coordinate. This procedure is formalized mathematically as:

$$\mathcal{R}^1 = \begin{cases} 1, & \text{if } p_i^e \sim p_{i,j}^r, \\ 0, & \text{if } p_i^e \not\sim p_{i,j}^r, \end{cases} \quad s_{i,j} = 1 + \mathcal{R}^1. \quad (1)$$

$$\mathcal{R}^2 = \begin{cases} 1, & \text{if } y_{i,j}^r = \min \{y_{i,p}^r \mid s_{i,p} = 2, 0 < p < m-1\}, \\ 0, & \text{otherwise} \end{cases}, \quad (2)$$

Let \hat{p}_i^r denote the point with the smallest y-coordinate in \mathcal{R}^2 , with its corresponding score \hat{s}_i . The application of the aforementioned rules generates a set of tuples, recorded as $(p_i^e, \hat{p}_i^r, \hat{s}_i)$. The endpoint p_i^e associated with the highest score is designated as P_h . In cases where multiple endpoints share the maximum score, the endpoint with the smallest y-coordinate is selected as the final P_h .

Target Point Estimation. TRACE embeds information by moving the handle point P_h to the corresponding point P_t . In the previous part, we thoroughly

describe the selection process of P_h . We hereby elaborate on the specific methodology for determining the corresponding P_t .

Assuming the relative distance between P_h and P_r along the λ -axis is denoted as $\Delta(P_h, P_r)$, where λ -axis can be modeled as follows:

$$\lambda\text{-axis is } \begin{cases} \text{X-axis,} & d_x \leq d_y \\ \text{Y-axis,} & d_x > d_y \end{cases}, \quad (3)$$

Here, d_x and d_y can be calculated via

$$d_x = |x_h - x_r|, \quad d_y = |y_h - y_r|, \quad (4)$$

where (x_h, y_h) , (x_r, y_r) are the coordinates of P_h and P_r , respectively, and $\Delta(P_h, P_r) = \min\{d_x, d_y\}$. To embed a bit value of 0, if $\Delta(P_h, P_r) > T_{\text{embed}}$, P_h is relocated to ensure $\Delta(P_t, P_r) \leq T_{\text{embed}}$. If $\Delta(P_h, P_r) \leq T_{\text{embed}}$ already, no repositioning is needed, thus avoiding unnecessary distortion. To embed a bit value of 1, P_h is relocated if $\Delta(P_h, P_r) \leq T_{\text{embed}}$ to ensure $\Delta(P_t, P_r) > T_{\text{embed}}$; otherwise, no adjustment is required.

Since P_t is relocated from P_h , we need to ensure that P_h maintains its identity from the embedding stage to the extraction stage when determining the position of P_t . Otherwise, synchronization errors may occur, compromising message recovery, *e.g.*, if the y-coordinate of P_h increases during embedding and exceeds that of other endpoints p_i^e within the triplet $(p_e^i, \hat{p}_r^i, \hat{s}^i)$ sharing the same score, the decoder may mistakenly treat an unmoved p_i^e as P_h .

To address this problem, we analyze the computation of P_t based on the embedded bit value (0 or 1). When the hidden bit is 0, P_t 's position depends on both the stroke direction containing P_h and the direction from P_h to P_r , represented by \mathcal{V} and \mathcal{H} , respectively. To calculate \mathcal{V} , we first construct a circle centered at P_h with radius r_h , as illustrated by the blue dashed circle in Fig. 2. Designating the intersection of this circle with I_{ske} as P_k with coordinates (x_k, y_k) , \mathcal{V} can be computed as

$$\mathcal{V} = (\mathcal{V}_x, \mathcal{V}_y) = (x_h - x_k, y_h - y_k). \quad (5)$$

Similarly, the vector \mathcal{H} is calculated as:

$$\mathcal{H} = (\mathcal{H}_x, \mathcal{H}_y) = (x_r - x_h, y_r - y_h). \quad (6)$$

Then, the coordinate (x_t, y_t) of P_t moved a distance \mathcal{D} can be expressed as:

$$x_t = x_h + \mathcal{D} \times \frac{\mathcal{V}_x}{\|\mathcal{V}\|} \times \text{sgn}(\mathcal{H}_x), \quad y_t = y_h + \mathcal{D} \times \frac{\mathcal{V}_y}{\|\mathcal{V}\|} \times \text{sgn}(\mathcal{H}_y), \quad (7)$$

where \mathcal{D} is defined in Eq. (8), and $\text{sgn}(\cdot)$ is a sign function.

$$\mathcal{D} = \begin{cases} |x_h - x_r| / |\mathcal{V}_x|, & \text{if } \lambda\text{-axis is X-axis} \\ |y_h - y_r| / |\mathcal{V}_y|, & \text{if } \lambda\text{-axis is Y-axis} \end{cases}. \quad (8)$$

When the embedding bit is 1, it is necessary to increase $\Delta(P_h, P_r)$ along λ -axis to complete the embedding process. The calculation for (x_t, y_t) is similar to the

aforementioned steps. We simply need to multiply $\text{sgn}(x)$ in Eq. (7) by -1 to indicate that P_h is moving away from P_r .

Beyond the above cases, additional scenarios warrant further analysis. When the λ -axis corresponds to the x -axis and $\Delta(P_h, P_r) = 0$, we designate that P_h moves along the direction of stroke elongation. When λ -axis aligns with the y -axis and $\Delta(P_h, P_r) = 0$, we calculate the angle θ between \mathbf{V} and the positive x -axis using Eq. (9).

$$\theta = \arccos \frac{\mathcal{V}_x}{\|\mathbf{V}\|}, \theta \in [0, 2\pi). \quad (9)$$

When $0 \leq \theta < \pi$, we increase $\Delta(P_h, P_r)$ by elongating the stroke; otherwise, we shorten it. Fig. 3 illustrates the moving direction of P_h corresponding to different intervals of θ . As shown in the blue box of Fig. 3, we first calculate \mathbf{V} using an auxiliary circle, then derive angle θ_1 from \mathbf{V} . Since $\theta_1 < 180^\circ$, we move P_h along \mathbf{V} towards the upper right. We can observe that the y -coordinate of P_t is smaller than the y -coordinate of P_h , which ensures the identity of P_h .

Mask Drawing Module. After obtaining the handle points and target points, we can construct the mask \mathcal{M} . In general, it is a binary image of size $H \times W$, where the editing region is represented by a ‘white rectangle’ (with a pixel value 255), *i.e.*, $\Omega = \{(x, y) : \Gamma_{\text{left}} - \sigma \leq x \leq \Gamma_{\text{right}} + \sigma, \Gamma_{\text{top}} - \sigma \leq y \leq \Gamma_{\text{right}} + \sigma\}$, where $\sigma \in \mathbb{Z}^+$. Specifically, taking the case where the λ -axis corresponds to the x -axis as an example, we first compute Γ_{left} and Γ_{right} via:

$$\Gamma_{\text{left}} = \min(x_h, x_t), \Gamma_{\text{right}} = \max(x_h, x_t). \quad (10)$$

Then, we extract a candidate area \mathcal{M}_c from I_{cover} , defined by a four-tuple $(0, \Gamma_{\text{left}}, H, \Gamma_{\text{right}} - \Gamma_{\text{left}})$ that specifies its top-left corner $(0, \Gamma_{\text{left}})$ and its height and width $(H, \Gamma_{\text{right}} - \Gamma_{\text{left}})$, to calculate Γ_{top} and Γ_{bottom} . The detailed calculation process is shown in Appendix E. Thus, we have obtained Γ_{top} , Γ_{bottom} , Γ_{left} , and Γ_{right} . Although we aim to minimize the mask size to reduce interference with the original image, excessively small masks may compromise the diffusion process, potentially producing outputs identical to the original image. Consequently, we expand \mathcal{M} by extending each boundary by a distance of σ , enlarging the mask area and improving diffusion quality.

3.3 Guided Diffusion Encoding

After obtaining the handle point P_h , the target point P_t , and the mask \mathcal{M} , we exploit DragDiffusion to move P_h to P_t . The process involves three key phases. Initially, DragDiffusion fine-tunes the diffusion model’s UNet with LoRA to better capture the features of the original image, enhancing identity consistency

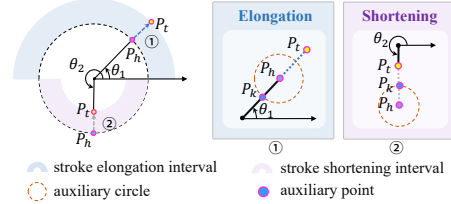


Fig. 3: Illustration the direction of P_h movements corresponding to its stroke in various orientations.

throughout the editing process. Following this, we apply DDIM inversion to I_{cover} to generate an initial diffusion latent that serves as the foundation for latent optimization. This optimization, guided by P_h and P_t , iteratively applies motion supervision and point tracking until the handle point aligns with its target. Finally, DragDiffusion implements reference-latent control during denoising by replacing the key and value vectors of the self-attention in the edited latent with those from the initial latent, thereby directing attention toward consistent features and textures.

DragDiffusion controls the update of the latent z_t (the result of the t -th step of DDIM inversion) via the motion supervision loss L_{ms} . However, our experiments (in Section 4.3) reveal that content generated within the mask tends to cause significant changes in local shapes. As such, to satisfy invisibility requirements, we introduce a local consistency loss L_{lc} . Denoting the feature vector at pixel location P_h as $G_{P_h}(\cdot)$, the loss at the k -th iteration is given by:

$$L_{lc}(\hat{z}_t^k) = \sum_{q \in \Omega} \|G_{q+d}(\hat{z}_{t-1}^k) - \text{sg}(G_q(\hat{z}_{t-1}^0))\|_1, \quad (11)$$

$$L(\hat{z}_t^k) = L_{ms}(\hat{z}_t^k) + \eta L_{lc}(\hat{z}_t^k), \quad (12)$$

where \hat{z}_t^k is the latent variable at step t after the k -th update, $\text{sg}(\cdot)$ is the stop-gradient operator, vector $d = h^k - h^0$ denotes the displacement vector, where h^k is the handle point at the k -th motion supervision iteration, Ω is the editing region defined by MDM, and η is weighting coefficient.

3.4 Masked Region Replacement

In our experiments (Section 4.3), we observe that DragDiffusion may cause feature alterations beyond the target region. To preserve the original features outside the edited region, we propose a masked region replacement method that replaces the content within the masked region of I_{cover} with corresponding content from the generated image. With this single step, information embedding is achieved while minimizing the impact on the original character.

3.5 Document Embedding and Extraction

The embedding procedure operates through two distinct mechanisms to ensure efficiency and generalization across typographies. For common characters, a pre-computed codebook is constructed prior to embedding, enabling rapid substitution of standard characters with their encoded counterparts. For unfamiliar styles or characters absent from the codebook, encoded representations are generated dynamically, enabling immediate encoding without additional model training or manual intervention.

Once we obtain the document with the embedded information, we implement the following extraction procedure. First, we segment individual characters using the CRAFT algorithm [2], following the approach adopted in AutoStegaFont.

Then, we apply the Movement Probability Estimator (MPE) to the structural representation of each character to identify P_h and P_r and calculate the distance $\Delta(P_h, P_r)'$ between these two points. The extraction decision follows a simple threshold rule: if $\Delta(P_h, P_r)' > T_{\text{embed}}$, we extract a bit value of ‘1’; otherwise, a bit of ‘0’ is extracted.

4 Experiment

4.1 Main Settings

Datasets. We conduct our main experiments on English and Chinese fonts. For English, we select Calibri, Arial, and Times New Roman (TNR); for Chinese, SimSun and SimHei are employed. For both English and Chinese fonts, we test six font sizes (in pt): {12, 16, 20, 24, 28, 36}. Additionally, we test TRACE on handwritten and artistic fonts to demonstrate its generalizability across diverse typographic styles. We further evaluate TRACE’s applicability to other foreign languages and mathematical formulas, with detailed results provided in Appendix G.1-G.2.

Baseline Selection. In main experiments, we compare TRACE with the state-of-the-art (SOTA) font-based document hiding method AutoStegaFont (ASF) [29] on the datasets described above. We also compare TRACE with two image-based methods, StegaStamp [24] and IHA [30], on document images, with visual analysis presented in Appendix K.1. To ensure a fair evaluation, we maintain consistent experimental equipment (*e.g.*, printers, scanners) and environmental conditions across all methods. More implementation details are in Appendix A.

Settings for Document Hiding. In our method, the parameter η in Eq. (12) is set to 0.003, and T_{embed} is set to 10. When the shortest edge of the original image is 512, τ and σ are set to 80 and 10, respectively. Their values are adjusted based on the image size. We adopt DragDiffusion with the same parameters as specified in [20]. As for ASF, we follow the same settings described in [29] and train on multiple fonts to generate character codebooks.

Evaluation Metrics. We evaluate robustness using average extraction accuracy (ACC), which measures the percentage of correctly extracted bits, with higher values indicating stronger robustness. To assess stealthiness, we adopt two widely used image quality metrics: Peak Signal-to-Noise Ratio (PSNR) and Structural Similarity Index (SSIM) [25], with higher values corresponding to better visual imperceptibility. Efficiency-related discussions are detailed in Appendix F.

4.2 Main Results

Performance of Robustness. We conduct a comprehensive evaluation of TRACE’s robustness against various real-world distortions compared to ASF [29], with results recorded in Tab. 1- 3. TRACE consistently outperforms ASF across all testing conditions, even achieving error-free extraction in some cases.

Table 1: Robustness against Screenshots across varying character sizes. Best results are in **boldface**.

Font	Method	Screenshots					
		12pt	16pt	20pt	24pt	28pt	36pt
Arial	ASF	85.83	91.67	90.00	87.50	88.33	82.50
	TRACE	96.67	97.50	99.17	100	100	100
TNR	ASF	70.83	77.50	72.50	69.17	74.17	80.83
	TRACE	92.50	92.50	95.00	97.50	100	100
Calibri	ASF	95.00	95.83	96.67	98.33	97.50	100
	TRACE	97.50	99.17	99.17	100	100	100
SimSun	ASF	86.67	87.50	90.83	91.67	92.50	93.33
	TRACE	90.83	91.67	95.00	95.83	95.83	97.50
Simhei	ASF	91.67	92.50	94.17	95.83	97.50	98.33
	TRACE	92.50	95.83	96.67	97.50	97.50	99.17

Table 3: Robustness against Print-camera captures across varying sizes. Best results are in **boldface**.

Font	Method	Print Camera					
		12pt	16pt	20pt	24pt	28pt	36pt
Arial	ASF	66.67	70.83	76.67	77.50	72.50	80.00
	TRACE	95.83	96.67	98.33	98.33	99.17	100
TNR	ASF	65.83	75.00	71.67	70.83	77.50	75.83
	TRACE	90.00	91.67	94.17	94.50	98.33	98.33
Calibri	ASF	71.67	72.50	75.83	69.17	71.67	72.50
	TRACE	96.67	97.50	97.50	99.17	100	100
SimSun	ASF	70.83	75.83	73.33	75.00	74.17	76.67
	TRACE	85.83	86.67	89.17	91.67	94.17	96.67
Simhei	ASF	77.50	72.50	76.67	79.17	83.33	85.83
	TRACE	90.00	90.83	93.33	95.00	95.83	96.67

This performance advantage is particularly pronounced for smaller font sizes and challenging print-scan and print-camera scenarios. Fig. 5 reveals that ASF’s limited robustness stems from its reliance on edge pixel manipulation, which is highly vulnerable to distortions. For instance, screenshots blur text edges, while printing introduces substantial noise along edges. In contrast, TRACE embeds watermarks through subtle structural adjustments that preserve the core character geometry despite edge pixel degradation. Note that both TRACE and ASF can correctly extract information without attacks.

We compare our method with Stegastamp [24] and IHA [30] on Calibri documents, both of which support cross-media transmission of text images. Table 4 reports quantitative results on robustness and invisibility. TRACE consistently achieves the best performance across all metrics, demonstrating superior robustness and invisibility. Visual comparisons are provided in Appendix K.1.

Given that photographing paper documents is common practice, we evaluated robustness under varying shooting distances and angles, as shown in Fig. 4. The left graph shows that TRACE maintains high accuracy (> 80%) even as the shooting angle increases to 60°, while ASF’s perfor-

Table 2: Robustness against Print-scan across varying character sizes. Best results are in **boldface**.

Font	Method	Print Scans					
		12pt	16pt	20pt	24pt	28pt	36pt
Arial	ASF	80.83	68.33	70.83	72.50	70.00	76.67
	TRACE	95.83	97.50	99.17	99.17	100	100
TNR	ASF	64.17	72.50	79.17	68.33	79.17	72.50
	TRACE	92.50	94.17	95.83	97.50	99.17	99.17
Calibri	ASF	73.33	77.50	75.00	70.00	69.17	74.17
	TRACE	98.33	99.17	100	100	100	100
SimSun	ASF	75.83	75.00	74.17	75.83	76.70	78.33
	TRACE	89.17	91.67	94.17	95.00	96.67	98.33
Simhei	ASF	77.50	87.50	84.17	85.00	88.33	87.50
	TRACE	91.67	92.50	95.00	96.67	97.50	98.33

Table 4: Invisibility and Robustness Comparison of TRACE and baselines on document images, evaluating robustness to screenshots, print-scan, and print-camera. Best results are in **boldface**.

Method	Stegastamp	IHA	TRACE
Screenshot	100	84.58	100
Print-scan	98.54	84.29	99.05
Print-camera	98.12	83.94	98.75
PSNR	27.19	29.60	33.34
SSIM	0.8986	0.9910	0.9962

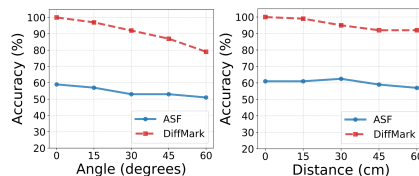
**Fig. 4:** Robustness against Print-camera with varying viewpoint and distance.

Table 5: PSNR and SSIM of TRACE and ASF, with best ACC marked in **boldface**.

	Method	Arial	TNR	Calibri	Simsun	Simhei
PSNR \uparrow	ASF	26.56	27.29	27.46	30.34	26.23
	TRACE	36.76	36.51	32.38	40.98	40.05
SSIM \uparrow	ASF	0.984	0.986	0.985	0.989	0.986
	TRACE	0.996	0.995	0.995	0.998	0.998

Table 6: Invisibility and Robustness of TRACE on handwritten to artistic fonts, evaluating robustness to screenshots, print-scan, and print-camera.

Method	Screenshots	Print-scan	Print-camera	PSNR	SSIM
Handwritten	94.43	93.17	91.67	38.20	0.996
Artistic	97.27	94.77	92.93	41.37	0.995

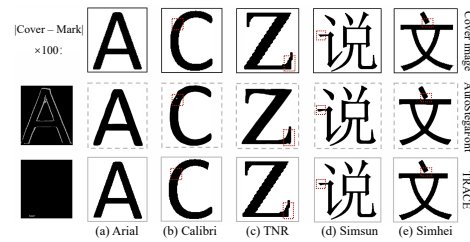
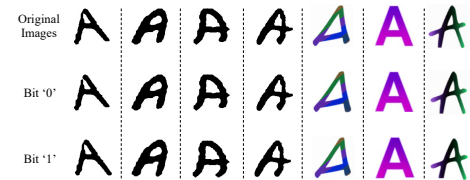
mance declines to approximately 50%. The right graph shows that TRACE sustains consistently high accuracy ($> 90\%$) across different shooting distances (20-60 cm), whereas ASF exhibits lower performance (approximately 60%) that slightly decreases with distance.

Performance of Imperceptibility.

Fig. 5 presents a comparison of encoded images generated by our TRACE, and ASF. The encoded image produced by TRACE demonstrates virtually imperceptible differences from the original image, with the residual image appearing almost completely black. In contrast, ASF’s encoded images display noticeable alterations along the edges, clearly visible in the residual image. The letter “C” in particular exhibits a hollowing effect in the ASF encoding. Quantitatively, TRACE achieves superior PSNR and SSIM metrics across both Chinese and English fonts, as detailed in Tab. 5.

Performance of Generalizability.

We embed both 0-bit and 1-bit data into diverse handwritten and artistic fonts. As shown in Fig. 6, TRACE demonstrates strong generalizability across various font styles. We further assess the robustness and invisibility of TRACE on these font types, with results presented in Table 6. We can see that TRACE achieves superior performance in both robustness and invisibility, striking a favorable balance among generalizability, robustness, and invisibility, which represents a significant advancement over previous methods.

**Fig. 5:** Visual comparisons of encoded images of our TRACE and the comparison method [29].**Fig. 6:** Generalizability of our TRACE from handwritten to artistic fonts.

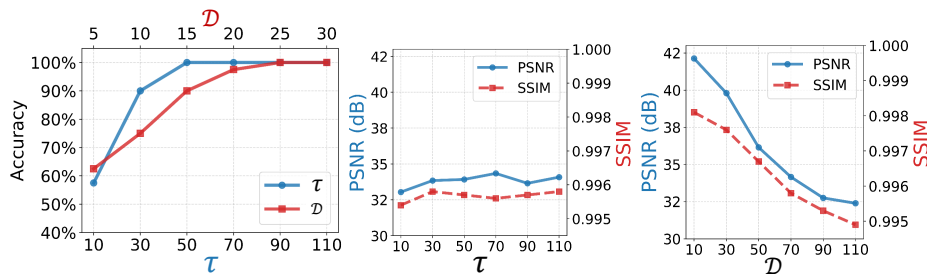


Fig. 7: Hyper-parameter Sensitivity Analysis: Impact of \mathcal{D} and τ on Watermarking Robustness (ACC) and Imperceptibility (PSNR, SSIM).

4.3 Ablation Study

Effects of Parameters \mathcal{D} and τ . The hyper-parameter \mathcal{D} controls the degree of handle point movement. If \mathcal{D} is too small, it may inadequately guide DragDiffusion in generating encoded images. Conversely, excessive \mathcal{D} values can produce overly noticeable movements, compromising invisibility. As shown in Fig. 7, except for these extreme cases, TRACE achieves an optimal balance between robustness and invisibility, offering a broad effective implementation range. Regarding hyper-parameter τ , a too small τ may cause a mismatch between P_r values of P_h before and after movement. However, as shown in Fig. 7, our method’s invisibility is not sensitive to variations in τ . As such, a wide range of τ can be selected for TRACE.

Effects of MPE and TPE. Recall that MPE aims to select the handle points and TPE determines the target points. To verify their effectiveness, we replace them with a random selection and conduct four experiments (e.g., Cases 1-4), as shown in Tab. 7.

Table 7: Ablation study on MPE and TPE. (✗: random point selection operation, ✓: MPE or TPE operation).

Design Setting	Setting 1	Setting 2	Setting 3	Setting 4 (Ours)
MPE	✗	✓	✗	✓
TPE	✗	✗	✓	✓
ACC	49.95	68.75	53.50	100

With both MPE and TPE active, extraction is error-free. MPE alone achieves limited accuracy due to probabilistic encoder-decoder synchronization. In the remaining two cases, accuracy approaches 50%, indicating random decoding. To further validate the design of MPE, we perform ablation studies on each of its scoring rules, demonstrating their individual necessity. Results are provided in Appendix D.

Effects of L_{lc} Loss. This loss is designed to enhance consistency of content in the masked area before and after embedding. As shown in Fig. 8, the L_{lc} loss significantly optimizes shape preservation in the masked region, rendering it virtually indistinguishable from the original image.

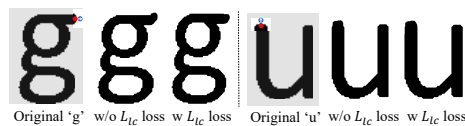
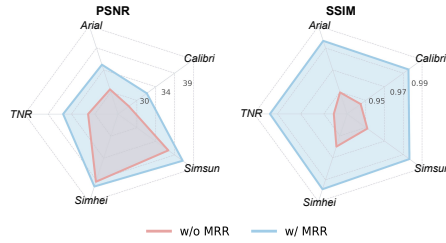


Fig. 8: Ablation study on L_{lc} loss, taking lowercase letters ‘g’ and ‘u’ in Calibri as examples.

Table 8: The robustness of our TRACE against structure morphing attack of varying strengths and font sizes.

Strength	12pt	16pt	20pt	24pt	28pt	36pt
Light	97.83	98.56	98.91	99.12	99.54	99.96
Strong	96.54	97.21	97.89	98.35	98.92	99.74

Effects of MRR. As shown in Fig. 9, MRR significantly enhances imperceptibility. Specifically, we observe varying degrees of improvement in PSNR and SSIM across different fonts, which can be attributed to MRR’s ability to embed data locally without affecting other regions of the image.

**Fig. 9:** Ablation study on MRR across various fonts in 12pt.

4.4 The Resistance to Adaptive Attacks

In this section, we consider adaptive attacks where adversaries understand our watermarking principle but lack knowledge of specific embedding parameters. Given that our method modifies character structures for watermark embedding, adversaries may attempt to disrupt extraction by applying perturbations to character geometries. We assess this threat by simulating structure morphing attacks through elastic deformations of character strokes, which subtly alter stroke contours and angles without compromising semantic identity. As shown in Table 8, TRACE demonstrates robust performance against both light and strong structure morphing attacks across various font sizes. These results confirm that TRACE maintains high extraction accuracy even when adversaries deliberately manipulate character structures, validating its effectiveness in practical adversarial scenarios. In addition, we further assess TRACE’s robustness against additional adaptive scenarios in Appendix H, such as common image processing, partial interception, and letter comparison.

5 Conclusion

We presented TRACE, a structure-based document hiding framework that leverages diffusion models to embed data via subtle modifications to character structures. TRACE comprises three key components: adaptive diffusion initialization, guided diffusion encoding, and masked region replacement. Extensive experiments verified TRACE’s superior cross-media robustness, multi-font and multi-language generalizability, high imperceptibility, and resilience against adaptive attacks. We hope our TRACE can provide new insights into document hiding, to facilitate trustworthy sharing and attribution of documents.

References

1. Abdelnabi, S., Fritz, M.: Adversarial watermarking transformer: Towards tracing text provenance with data hiding. In: 2021 IEEE Symposium on Security and Privacy (SP). pp. 121–140. IEEE (2021) [1](#)
2. Baek, Y., Lee, B., Han, D., Yun, S., Lee, H.: Character region awareness for text detection. In: CVPR (2019) [9](#)
3. Brassil, J.T., Low, S., Maxemchuk, N.F.: Copyright protection for the electronic distribution of text documents. *Proceedings of the IEEE* **87**(7), 1181–1196 (1999) [4](#), [9](#)
4. Brassil, J.T., Low, S., Maxemchuk, N.F., O’Gorman, L.: Electronic marking and identification techniques to discourage document copying. *IEEE Journal on Selected Areas in Communications* **13**(8), 1495–1504 (1995) [4](#)
5. Cao, Z., Hidalgo, G., Simon, T., Wei, S.E., Sheikh, Y.: Openpose: Realtime multi-person 2d pose estimation using part affinity fields. *IEEE TPAMI* **43**(1), 172–186 (2019) [5](#)
6. Dathathri, S., See, A., Ghaisas, S., Huang, P.S., McAdam, R., Welbl, J., Bachani, V., Kaskasoli, A., Stanforth, R., Matejovicova, T., et al.: Scalable watermarking for identifying large language model outputs. *Nature* **634**(8035), 818–823 (2024) [4](#), [9](#)
7. He, X., Xu, Q., Zeng, Y., Lyu, L., Wu, F., Li, J., Jia, R.: Cater: Intellectual property protection on text generation apis via conditional watermarks (2022) [4](#), [9](#)
8. Ho, J., Jain, A., Abbeel, P.: Denoising diffusion probabilistic models (2020) [4](#)
9. Hu, R., Zhang, J., Zhao, S., Lukas, N., Li, J., Guo, Q., Qiu, H., Zhang, T.: Mask image watermarking (2025) [1](#)
10. Huang, D., Yan, H.: Interword distance changes represented by sine waves for watermarking text images **11**(12), 1237–1245 (2001) [4](#)
11. Huang, X., Wang, H.: Robust text watermarking based on average skeleton mass of characters against cross-media attacks. *Journal of Visual Communication and Image Representation* **104**, 104300 (2024) [1](#), [4](#), [9](#)
12. Kirchenbauer, J., Geiping, J., Wen, Y., Katz, J., Miers, I., Goldstein, T.: A watermark for large language models. In: ICML (2023) [4](#), [9](#)
13. Li, L., Zhang, H.J., Meng, J.L., Lu, Z.M.: Robust pdf watermarking against print–scan attack. *Sensors* **23**(17), 7365 (2023) [4](#), [9](#)
14. Ling, H., Kreis, K., Li, D., Kim, S.W., Torralba, A., Fidler, S.: Editgan: High-precision semantic image editing (2021) [4](#)
15. Liu, H., Xu, C., Yang, Y., Zeng, L., He, S.: Drag your noise: Interactive point-based editing via diffusion semantic propagation. In: CVPR (2024) [4](#)
16. Meng, J., Li, Y., Lu, Z., He, Z., Luo, H., Zhang, T.: Coremark: Toward robust and universal text watermarking technique. *arXiv preprint arXiv:2506.23066* (2025) [2](#), [4](#)
17. Nichol, A.Q., Dhariwal, P.: Improved denoising diffusion probabilistic models. In: ICML (2021) [4](#)
18. Qi, W., Guo, W., Zhang, T., Liu, Y., Guo, Z., Fang, X.: Robust authentication for paper-based text documents based on text watermarking technology. *Mathematical biosciences and engineering* **16**(4), 2233–2249 (2019) [3](#), [5](#), [9](#)
19. Sander, T., Fernandez, P., Durmus, A., Furon, T., Douze, M.: Watermark anything with localized messages. In: ICLR (2025) [1](#)
20. Shi, Y., Xue, C., Liew, J.H., Pan, J., Yan, H., Zhang, W., Tan, V.Y., Bai, S.: Dragdiffusion: Harnessing diffusion models for interactive point-based image editing. In: CVPR (2024) [2](#), [4](#), [10](#), [7](#)

21. Shin, J., Choi, D., Park, J.: Instantdrag: Improving interactivity in drag-based image editing. In: SIGGRAPH (2024) [4](#), [5](#)
22. Sun, N., Zhao, C., Xie, S., Ling, H.: Invertedfontnet: Font watermarking based on perturbing style manifold. In: ICASSP (2024) [3](#)
23. Tan, L., Hu, K., Zhou, X., Chen, R., Jiang, W.: Print-scan invariant text image watermarking for hardcopy document authentication. *Multimedia Tools and Applications* **78**, 13189–13211 (2019) [4](#)
24. Tancik, M., Mildenhall, B., Ng, R.: Stegastamp: Invisible hyperlinks in physical photographs. In: CVPR (2020) [10](#), [11](#), [8](#)
25. Wang, Z., Bovik, A.C., Sheikh, H.R., Simoncelli, E.P.: Image quality assessment: from error visibility to structural similarity. *IEEE TIP* **13**(4), 600–612 (2004) [10](#)
26. Wu, M., Liu, B.: Data hiding in binary image for authentication and annotation. *IEEE TMM* **6**(4), 528–538 (2004) [2](#), [4](#), [6](#)
27. Xiao, C., Zhang, C., Zheng, C.: Fontcode: Embedding information in text documents using glyph perturbation. *ACM TOG* **37**(2), 1–16 (2018) [2](#), [3](#), [5](#), [7](#), [9](#)
28. Yang, X., Zhang, J., Chen, K., Zhang, W., Ma, Z., Wang, F., Yu, N.: Tracing text provenance via context-aware lexical substitution. In: AAAI (2022) [4](#), [9](#)
29. Yang, X., Zhang, J., Fang, H., Liu, C., Ma, Z., Zhang, W., Yu, N.: Autostegafont: synthesizing vector fonts for hiding information in documents. In: AAAI (2023) [2](#), [3](#), [4](#), [10](#), [12](#), [5](#), [7](#), [8](#), [11](#)
30. Yang, X., Zhang, W., Fang, H., Ma, Z., Yu, N.: Language universal font watermarking with multiple cross-media robustness. *Signal Processing* **203**, 108791 (2023) [4](#), [10](#), [11](#), [7](#), [8](#), [9](#)
31. Yao, Y., Wang, C., Wang, H., Wang, K., Ren, Y., Meng, W.: Embedding secret message in chinese characters via glyph perturbation and style transfer (2024) [3](#)
32. Zhang, R., Hussain, S.S., Neekhara, P., Koushanfar, F.: {REMARK-LLM}: A robust and efficient watermarking framework for generative large language models. In: 33rd USENIX Security Symposium (2024) [1](#)
33. Zhang, Z., Han, L., Ghosh, A., Metaxas, D.N., Ren, J.: Sine: Single image editing with text-to-image diffusion models. In: CVPR (2023) [4](#)
34. Zhao, H., Ma, X.S., Chen, L., Si, S., Wu, R., An, K., Yu, P., Zhang, M., Li, Q., Chang, B.: Ultraedit: Instruction-based fine-grained image editing at scale (2024) [4](#)
35. Zou, D., Shi, Y.Q.: Formatted text document data hiding robust to printing, copying and scanning. In: ISCAS (2005) [4](#)

Appendix

A More Implementation Details

English Dataset. The English dataset comprises three fonts: Arial, Times New Roman, and Calibri. For each font at each size, we create 60 text images containing both uppercase and lowercase letters, with character repetition as needed to achieve the required sample size. While image dimensions vary across font sizes, character composition remains consistent. To evaluate each character’s data-carrying capacity and robustness, we embed both ‘0’ and ‘1’ bits into the 60 images, generating 120 data samples for extraction accuracy assessment. This procedure is repeated for each font across various sizes using both TRACE and AutoStegaFont methods, with results presented in Tab. 1- 3.

Chinese Dataset. The Chinese dataset incorporates two widely adopted fonts: SimSun and SimHei. For each font, we generate the 60 most frequently used Chinese characters using ChatGPT. At each font size, we embed both ‘0’ and ‘1’ bits into these 60 characters, producing 120 data samples for extraction accuracy calculation.

Equipment. The printer and scanner used in the experiment are HP LaserJet Pro MFP M132nw and Epson V30 SE, both with a resolution of 600 dpi. The shooting device is a Xiaomi 14 mobile phone.

B More Details of Keypoint Detection

Fig. A displays the heatmaps generated by the keypoint extraction network, where pixel values indicate the probability of a location belonging to a specific joint class. In our configuration, the first channel represents endpoints, the second channel represents junction points, and the third channel corresponds to the background.

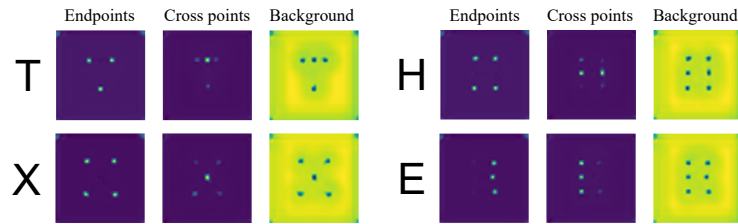


Fig. A: Three heatmaps output by the keypoint extraction network, including an endpoint heatmap, a junction point heatmap, and a background heatmap.

Algorithm 1 Movement probability evaluator (MPE).

Input: E, C
Output: P_h and P_r

- 1: **for** $p_i^e \in E$ **do**
- 2: Generate R_i for the current p_i^e
- 3: **if** $\text{len}(R_i) = 0$ **then**
- 4: // If p_i^e has no reference point, the possibility of becoming P_h is 0.
 Set initial score $s_{i,j} \leftarrow 0$ for p_i^e
- 5: **else**
- 6: Set initial score $s_{i,j} \leftarrow 1$ for each $p_{i,j}^r \in R_i$
- 7: **for** $j \in \{1, \dots, \text{len}(R_i)\}$ **do**
- 8: // \mathcal{R}^1 : check the connectivity.
- 9: **if** p_i^e and $p_{i,j}^r$ are not on the same stroke **then**
- 10: $s_{i,j} \leftarrow s_{i,j} + 1$
- 11: **end if**
- 12: **end for**
- 13: // \mathcal{R}^2 : add one point to the $p_{i,j}^r$ with the smallest $y_{i,j}^r$ and a score of 2.
 $j_{\min} = \arg \min_j y_{i,j}^r, s_{i,j_{\min}} \leftarrow s_{i,j_{\min}} + 1$
- 14: // Choose the p_i^e with the highest score as the final reference point for the
 current p_i^e .
 $j_{\max} = \arg \max_j s_{i,j}$
 $\hat{s}_i \leftarrow s_{i,j_{\max}}, \hat{p}_r^i \leftarrow p_{j_{\max}}^r$
- 15: **end if**
- 16: **end for**
- 17: // Next, select the final P_h from E .
- 18: $i_{\max} = \arg \max_i \hat{s}_i$
- 19: $S_{\text{idx}} = \{i \mid \hat{s}_i = \hat{s}_{i_{\max}}\}$
- 20: **if** $\text{len}(S_{\text{idx}}) = 1$ **then**
- 21: $P_h \leftarrow p_{i_{\max}}^e, P_r \leftarrow \hat{p}_{i_{\max}}^r$
- 22: **else**
- 23: // If there are multiple maximum values, choose the p_i^e with the smallest
 y -coordinate as P_h .
 $\beta = \arg \min_{i \in S_{\text{idx}}} (p_i^e)_y$
 $P_h \leftarrow p_{\beta}^e, P_r \leftarrow \hat{p}_{\beta}^r$
- 24: **end if**
- 25: **return** P_h and its reference point P_r

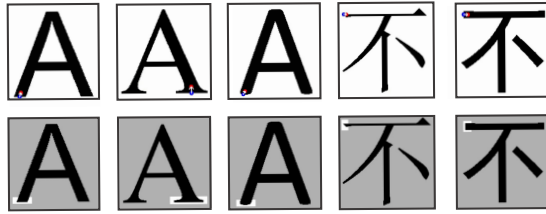


Fig. B: Examples of handle points and target points selected by MPE and TPE, respectively, and masks drawn by MDM.

C More Details of MPE

The proposed Movement Probability Evaluator (MPE) method is designed to automatically determine the handle point for each character, with its main steps discussed in Section 3.2. To facilitate a clearer understanding, we provide detailed pseudocode in Algorithm 1, which outlines the workflow and key computational steps of MPE. In addition, we provide some output examples of handle points picked by MPE in Fig. B, where the handle points are marked as blue dots. The red dots are the target points generated by the Target Point Estimation (TPE). For each example, we also present the corresponding masks generated by mask drawing module (MDM), as shown in the second row of Fig. B.

D Ablation Studies of MPE

In Section 4.3, we demonstrated that MPE is essential for TRACE. Specifically, MPE selects handle points using three rules. Here, we validate the necessity of each rule through additional ablation studies. The three rules are:

- **Rule 1:** Assign each endpoint an initial score of 1.
- **Rule 2:** For candidates scoring 1 after Rule 1, increment the score by 1 if the candidate and its reference point lie on different strokes.
- **Rule 3:** Among candidates with equal highest scores after Rule 2, the candidate with the smallest y-coordinate is assigned an additional score of 1, and this point is selected as the handle point.

Each rule progressively updates candidate scores, with MPE ultimately selecting the highest-scoring point as the handle point. To validate the necessity of each rule, we design three ablation experiments, each eliminating the effect of one rule on the final scoring:

- **w/o Rule 1:** Assign scores to junction points as well rather than restricting the initial scoring to endpoints only.
- **w/o Rule 2:** Remove the stroke connectivity constraint, treating all points equally.
- **w/o Rule 3:** Eliminate y-coordinate-based selection, randomly choosing among top-scoring candidates when multiple candidates share the highest score.

As shown in Table A, the full version of MPE achieves the best performance across all metrics. The **w/o Rule 1** experiment demonstrates that without proper initial endpoint scoring, structural disruption occurs, resulting in the lowest PSNR and ACC. The **w/o Rule 2** experiment reveals that ignoring stroke consistency leads to character invariance, causing embedding failure. Consequently, PSNR increases due to minimal perturbation, while ACC decreases drastically. The **w/o Rule 3** experiment shows that removing y-coordinate prioritization causes desynchronization between the encoder and decoder, compromising robustness. These findings collectively demonstrate the necessity and effectiveness of each proposed heuristic rule in MPE.

Table A: Ablation study on MPE scoring rules, failed cases (*i.e.*, PSNR < 30dB, SSIM < 0.95, and ACC < 85%) are marked in red.

Method	PSNR (dB) \uparrow	SSIM \uparrow	ACC (%) \uparrow
w/o Rule 1:	25.24	0.911	63.33
w/o Rule 2:	39.48	0.997	80.67
w/o Rule 3:	32.82	0.965	68.51
MPE (Ours)	32.10	0.962	100.00

E Detailed Calculation Process of Mask Drawing Module

After obtaining \mathcal{M}_c , which is defined by a four-tuple $(0, \Gamma_{\text{left}}, H, \Gamma_{\text{right}} - \Gamma_{\text{left}})$, we hereby illustrate how to calculate Γ_{top} and Γ_{bottom} . Assume that in I_{cover} , text is black (pixel value 0) and background is white (pixel value 255), we process each column of pixel sequence \mathcal{M}_c^i of \mathcal{M}_c by removing its first element to obtain a new sequence $\widetilde{\mathcal{M}}_c^i$, and appending a large value (*e.g.*, 254) to maintain the same length. We then compute the difference between \mathcal{M}_c^i and $\widetilde{\mathcal{M}}_c^i$ to obtain sequence ζ . The values of 255 in ζ mark the transitions from non-black to black pixels. We filter transition points occurring before y_h and store their indices in ζ_{255}^i . Let $\mathcal{K}_{\text{top}} = \{\kappa_{\text{top}}^i | i = 1, 2, \dots, \Gamma_{\text{right}} - \Gamma_{\text{left}}\}$ store the maximum value of ζ_{255}^i for each \mathcal{M}_c^i . If no values in ζ_{255}^i meet the criteria, we set κ_{top}^i to y_h ; otherwise, we select the largest value as κ_{top}^i . For Γ_{top} , it equals to $\min(y_h, y_t, \min(\mathcal{K}_{\text{top}}))$. Similarly, positions with a value of -255 in ζ represent the transitions from black to non-black pixels. We select transition points occurring after y_h and store their indices in ζ_{-255}^i . Let $\mathcal{K}_{\text{bottom}} = \{\kappa_{\text{bottom}}^i | i = 1, 2, \dots, \Gamma_{\text{right}} - \Gamma_{\text{left}}\}$ store the minimum value of ζ_{-255}^i for each \mathcal{M}_c^i . If the length of ζ_{-255}^i is 0, set $\kappa_{\text{bottom}}^i = y_h$; otherwise, assign the smallest value to κ_{bottom}^i . Γ_{bottom} is equals to $\max(y_h, y_t, \max(\mathcal{K}_{\text{bottom}}))$.

F Efficiency of TRACE

Given a real image with the resolution of 512×512 , the execution time of different stages in TRACE on a 4090 GPU is as follows: LoRA fine-tuning is around 30

seconds, latent optimization is around 1 minute depending on the magnitude of the hyper-parameter \mathcal{D} , the adaptive diffusion initialization is negligible comparing to previous steps (about 0.01 to 0.015 second), and the watermark extraction is extremely fast, taking approximately 0.005 second. The execution time of different stages in TRACE on an NVIDIA RTX 4090 GPU for a 512×512 resolution image is as follows: LoRA fine-tuning requires approximately 30 seconds, latent optimization takes around 1 minute (varying with the hyperparameter \mathcal{D} , adaptive diffusion initialization is negligible at 0.01-0.015 seconds, and watermark extraction is extremely efficient at approximately 0.005 seconds.

Arguably, in general, although efficiency is not the main focus of this paper, we hereby discuss several potential strategies to further improve our efficiency. Firstly, consistent with existing approaches [18, 27, 29], we can pre-compute a character codebook to mitigate runtime overhead. Under equivalent codebook conditions, our method demonstrates superior robustness and imperceptibility, as evidenced in Table 1-5. Secondly, our approach leverages DragDiffusion, a point-based image editing method, to subtly adjust character structures. As illustrated in Fig. 2, DragDiffusion operates independently from the rest of our pipeline, allowing users to optionally substitute it with more lightweight alternatives, such as InstantDrag [21], to achieve greater efficiency. To demonstrate this flexibility, we replaced DragDiffusion with InstantDrag, which significantly reduces the information embedding time to 0.704 seconds. However, since InstantDrag tends to produce larger structural displacements, invisibility slightly decreases, with PSNR dropping by approximately 0.7 dB and SSIM by 0.0002. Nevertheless, robustness remains largely consistent with DragDiffusion, demonstrating that our framework can flexibly trade off efficiency and imperceptibility without sacrificing watermarking reliability.

G Additional Generalizability Analysis

G.1 Generalizability to Other Languages

In the main manuscript, we evaluated TRACE on two Chinese fonts and three English fonts. To further assess its generalizability, we hereby additionally apply TRACE to fonts from other widely used languages, including Korean, Japanese, Russian, and Arabic. We exclude languages that use alphabetic systems similar to English (e.g., French and Spanish) from this analysis. As shown in Figure C, TRACE successfully embeds distinct bit information into characters across these languages while maintaining good invisibility.

G.2 Generalizability to Mathematical Formulas

Given that mathematical formulas frequently appear in academic and technical documents, we further examine TRACE’s adaptability to this type of content. We select three commonly used formulas as examples and embed both 0 and 1 bits into their constituent characters, as illustrated in Figure D. TRACE consistently embeds information across these formulas while maintaining strong visual invisibility.

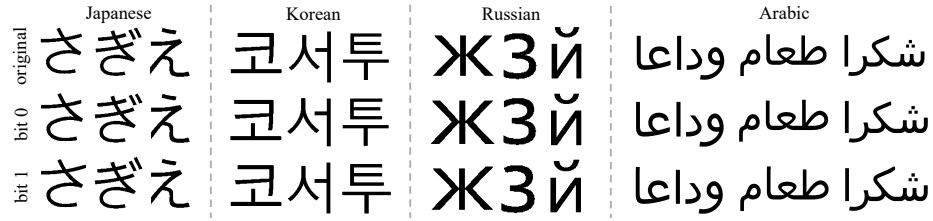


Fig. C: Examples of Japanese, Korean, Russian, and Arabic characters embedding '0' and '1' using the TRACE method.

original	$MSE = \frac{1}{N} \sum_{i=1}^N (y_i - \bar{y}_i)^2$	$H(X) = - \sum p(x) \log p(x)$	$C = 2 \times \pi \times r$
bit 0	$MSE = \frac{1}{N} \sum_{i=1}^N (y_i - \bar{y}_i)^2$	$H(X) = - \sum p(x) \log p(x)$	$C = 2 \times \pi \times r$
bit 1	$MSE = \frac{1}{N} \sum_{i=1}^N (y_i - \bar{y}_i)^2$	$H(X) = - \sum p(x) \log p(x)$	$C = 2 \times \pi \times r$

Fig. D: Generalizability in mathematical formulas, each character in every formula embeds 0 and 1 bits, respectively.

H The Resistance to More Adaptive Attacks

H.1 Resistance to Common Image Processing

If attackers lack knowledge of our method's design, they may eliminate the embedded information through common image processing. To evaluate resistance to such attacks, we apply Gaussian noise with a variance of 0.03 and a 3×3 Gaussian blur to 30 encoded character images in 12pt Calibri font. We then extract the embedded information from the attacked images and calculate the accuracy (ACC). The results show that the watermark extraction accuracy remains at 100% under both attacks, confirming that our method effectively withstands common image processing attacks.

H.2 Resistance to Letter Comparing

We admit that, due to the inherently sparse pixel distribution in text images, text-based watermarking methods may face a fundamental challenge: direct comparison between the encoded and original images may reveal watermark presence or leak embedded content. For instance, in font-based approaches employing fixed character codebooks, attackers could potentially infer embedded information through character-to-codebook matching. However, in most practical scenarios, the primary goal of an attacker is to forge authentication data to pass document validation tests [26]. To mitigate this threat, we employ a 128-bit secret key for message encryption prior to embedding. The cryptographic security of this approach is evident: the probability of successfully compromising a 128-bit key is 2^{-128} , which is computationally infeasible. Consequently, even if an

attacker manages to extract the ciphertext from the image, extracts the ciphertext from the image, they cannot decrypt the underlying plaintext or forge valid authentication information.

H.3 Resistance to Partial Interception

Attackers may only capture the content they are interested in. In this section, we evaluate TRACE’s resistance to such partial interception attacks. Typically, minimal data, such as an ID or name, is sufficient to indicate identity. TRACE embeds one bit per character, enabling repeated data hiding to resist partial interception. To demonstrate this capability, we evaluate the impact of both embedded bits and the number of consecutively selected words on average extraction accuracy. Tab. B shows the average accuracy over 10,000 extractions. As seen, with an appropriate amount of embedded information, repeated embedding ensures robustness. It is worth noting that attackers are unlikely to extract only a few words, as it would be meaningless.

Table B: Impact of embedded bits and consecutive word count on average extraction accuracy.

Number of words	5	10	15	20
8bit	97.78	100.00	100.00	100.00
16bit	59.76	99.62	100.00	100.00
32bit	0.37	61.16	99.03	100.00

I Potential Limitations and Future Directions

Firstly, TRACE primarily embeds information through the endpoints of character structures. For characters without endpoints (*e.g.*, ‘o’), information cannot be embedded. However, we argue that this limitation is mild, as such characters constitute only a small portion of the document, and we can always embed information using other characters. To further improve generalizability, we will design specific embedding rules for characters without keypoints in the future. Secondly, while LoRA fine-tuning in DragDiffusion [20] introduces additional time overhead, we have mitigated this limitation in Section F by demonstrating that DragDiffusion can be substituted with lightweight alternatives such as InstantDrag, significantly reducing embedding time to 0.704 seconds. Further efficiency optimizations remain a direction for future work.

J Discussions of OCR Attacks

Following prior works [27, 29, 30], this paper does not consider OCR-based attacks, as OCR fundamentally transforms the watermark carrier itself. Once the document is converted through OCR, the original digital carrier ceases to exist, making subsequent evaluation of watermark performance largely meaningless. In contrast, this paper aims to protect the document carrier itself rather than only the textual content.

Furthermore, OCR attacks are not universally applicable, as they fail in two important scenarios. First, OCR systems cannot faithfully reproduce stylized

fonts such as artistic or handwriting styles. Our method is, to the best of our knowledge, the first document watermarking scheme that generalizes to these font types, making it effective in settings where OCR-based attacks are inherently limited. Second, the authentication of officially sealed documents fundamentally depends on the physical presence of the seal. Even if OCR successfully extracts the textual content, the document cannot be verified without the original seal, rendering such attacks invalid in practice.

To the best of our knowledge, the only text watermarking techniques capable of withstanding OCR-based attacks are linguistic approaches that alter the original textual content. However, such alterations are typically infeasible in formal documents where content integrity is mandatory. Besides, as observed in [29], existing linguistic watermarking schemes cannot guarantee that the modified text remains fully semantically equivalent to the original.

K Extended Qualitative Analysis

K.1 Visual Comparison to Baselines

We conduct comparisons with the image watermarking method StegaStamp [24] and the information hiding approach (IHA) [30] in Section 4 of the main text. Fig. E presents a visual quality comparison of these document watermarking methods. As shown, StegaStamp introduces noticeable artifacts after information embedding, while IHA leaves overly visible traces that alter the original appearance of certain characters. In contrast, our method achieves superior performance by preserving character appearance with minimal perceptible changes.

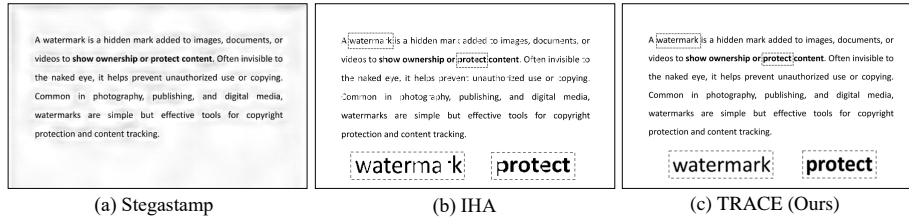


Fig. E: The visual effects of our method and the comparison methods.

K.2 Comparative Analysis of Existing Methods

In the main experimental section, we conduct quantitative comparisons with three representative methods [24, 29, 30]. However, other document watermarking methods are excluded from quantitative analysis due to their inherent limitations

and instead presented in a broader qualitative comparison in Tab. C. Part of the discussion in this section is inspired by the analysis in [30].

Specifically, as representative of font-based methods, [18,27] demonstrate robustness against cross-media transmission (*e.g.*, print-scan or screenshot). However, they suffer from limited generalizability. In particular, the diversity of hand-written and artistic fonts makes it difficult for font-based encoding schemes to handle all scenarios. Besides, these methods often fail when encountering unseen languages or formulaic symbols, as they typically rely on manually crafted character codebooks that are not easily extensible.

For image-based methods [11,13], information is embedded by inverting black and white pixels. As a result, they lack generalizability to artistic fonts, which are typically colorful and thus incompatible with such binary manipulations.

Format-based method [3] rely on layout-level manipulations. While they can be effective in controlled environments, camera-based attacks often introduce distortions (*e.g.*, altered spacing), which undermine the stability of embedding features and significantly affect robustness.

Linguistic-based approaches [6,7,12,28] embed information by modifying syntactic or semantic properties of the text. However, due to structural and semantic constraints, such substitutions are not supported in all languages. Moreover, these modifications typically alter the original content, thereby compromising semantic integrity and limiting their applicability in scenarios that require strict preservation of textual meaning, such as legal documents, medical records, or academic publications.

Table C: Qualitative comparison with related work from different perspectives.

Category	Method	Robustness			Generalizability				Integrity
		Print-scan	Print-camera	Screenshot	Handwritten	artistic	formula	Language-universality	
Font-based	[18,27]	✓	✓	✓	✗	✗	✗	✗	✓
Image-based	[11,13]	✓	✓	✓	✓	✗	✓	✓	✓
Format-based	[3]	✓	✗	✓	✓	✓	✓	✓	✓
Linguistic-based	[6,7,12,28]	✓	✓	✓	✗	✓	✗	✗	✗
TRACE (Ours)		✓	✓	✓	✓	✓	✓	✓	✓

L More Visual Cases

In this section, we make more qualitative comparisons between TRACE and AutoStegaFont in Fig. F-J. The results consistently show that our method achieves significantly better visual quality than AutoStegaFont. Furthermore, it is important to note that AutoStegaFont requires pre-training on the target font before encoding its characters, which introduces considerable complexity and inconvenience in practical applications.

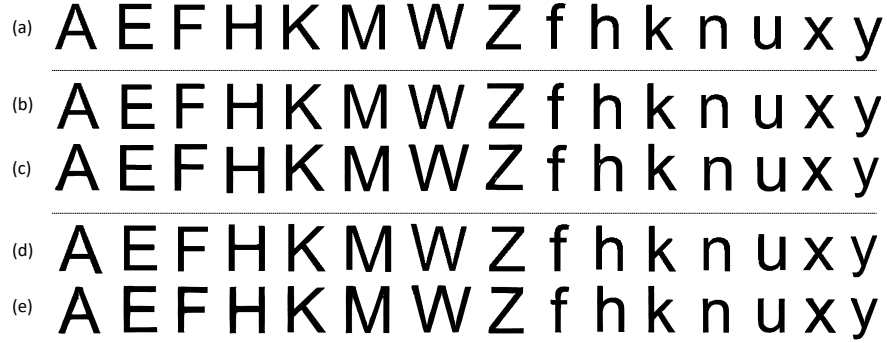


Fig. F: Visual comparisons of our TRACE and the comparison method AutoStegaFont [29] on encoded images of the Arial font, (a) original images, (b) encoded images embedding “0” by TRACE, (c) encoded images embedding “1” by AutoStegaFont, (d) encoded images embedding “1” by TRACE, (e) encoded images embedding “0” by AutoStegaFont.

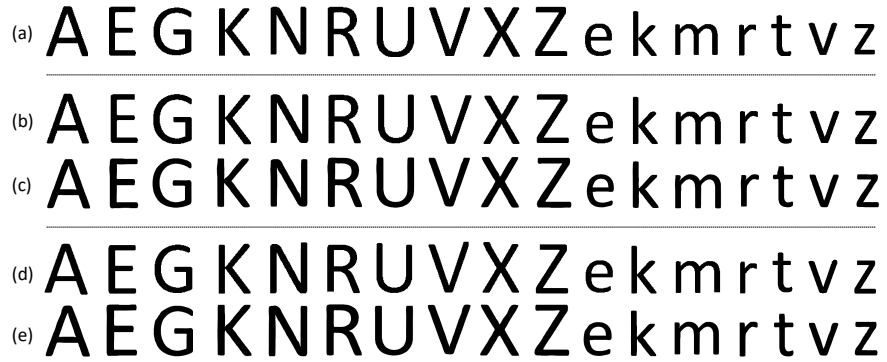


Fig. G: Visual comparisons of our TRACE and the comparison method AutoStegaFont [29] on encoded images of the Calibri font, (a) original images, (b) encoded images embedding “0” by TRACE, (c) encoded images embedding “1” by AutoStegaFont, (d) encoded images embedding “1” by TRACE, (e) encoded images embedding “0” by AutoStegaFont.

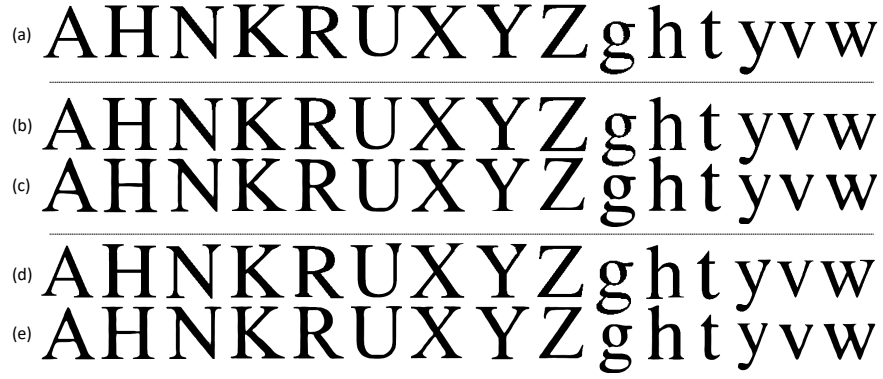


Fig. H: Visual comparisons of our TRACE and the comparison method AutoStegaFont [29] on encoded images of the Times New Roman font, (a) original images, (b) encoded images embedding “0” by TRACE, (c) encoded images embedding “1” by AutoStegaFont, (d) encoded images embedding “1” by TRACE, (e) encoded images embedding “0” by AutoStegaFont.

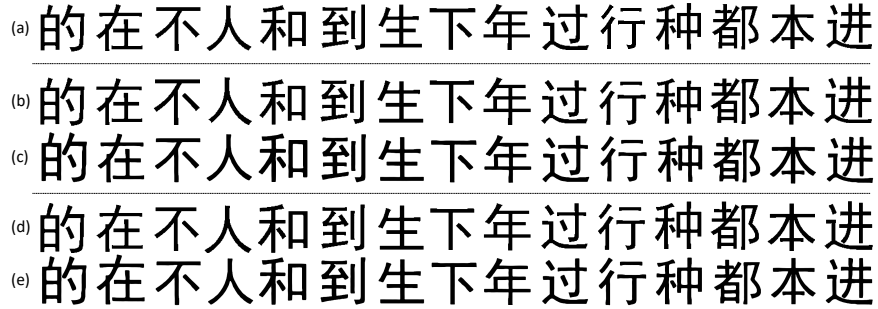


Fig. I: Visual comparisons of our TRACE and the comparison method AutoStegaFont [29] on encoded images of the Simhei font, (a) original images, (b) encoded images embedding “0” by TRACE, (c) encoded images embedding “1” by AutoStegaFont, (d) encoded images embedding “1” by TRACE, (e) encoded images embedding “0” by AutoStegaFont.

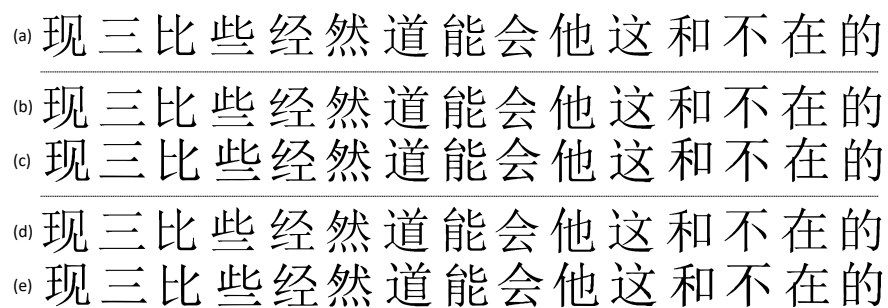


Fig. J: Visual comparisons of our TRACE and the comparison method AutoStegaFont [29] on encoded images of the Simsun font, (a) original images, (b) encoded images embedding “0” by TRACE, (c) encoded images embedding “1” by AutoStegaFont, (d) encoded images embedding “1” by TRACE, (e) encoded images embedding “0” by AutoStegaFont.